Nonlinear analysis of high-Reynolds-number flows over a buoyant axisymmetric body

Henry D. I. Abarbanel*
Department of Physics and Marine Physical Laboratory, Scripps Institution of Oceanography, University of California, San Diego, Mail Code 0402, La Jolla, California 92093-0402

Richard A. Katz
Naval Undersea Warfare Center Detachment New London, Code 33A, Building 2, New London, Connecticut 06320

Thomas Galib and Joan Cembrola
Naval Undersea Warfare Center Division Newport, 1176 Howell Street, Code 814, Newport, Rhode Island 02841-1708

Theodore W. Frison
Randle, Inc., P.O. Box 587, Great Falls, Virginia 22066
(Received 22 September 1993)

Data from experiments on the turbulent boundary layer around an axisymmetric vehicle rising under its own buoyancy are described in detail and analyzed using tools developed in nonlinear dynamics. Arguments are given that in this experiment the size of the wall mounted pressure sensors would make the data sensitive to the dynamics of about ten or so coherent structures in the turbulent boundary layer. Analysis of a substantial number of large, well sampled data sets indicates that the (integer) dimension of the embedding space required to capture the dynamics of the observed flows in the laminar regime is very large. This is consistent with there being no pressure fluctuations expected here and the signal being dominated by instrumental "noise." In a consistency check we find that data from the ambient state of the vehicle before buoyant rise occurs and data from an accelerometer mounted in the prow are also consistent with this large dimension. The time scales in those data are also unrelated to fluid dynamic phenomena. In the transition and turbulent regions of the flow we find the pressure fluctuation time scales to be consistent with those of the fluid flow (about 250 μsec) and determine the dimension required for embedding the data to be about 7–8 for the transitional region and about 8–9 for the turbulent regime. These results are examined in detail using both global and local false nearest-neighbor methods as well as mutual information aspects of the data. The results indicate that the pressure fluctuations are determined in these regimes by the coherent structures in the turbulent boundary layer. Applications and further investigations suggested by these results are discussed.

PACS number(s): 47.27.Jv, 02.50.−r, 64.10.+h

I. INTRODUCTION

Fluid flow over a rapidly moving body creates Tollmien-Schlichting (TS) waves which develop from the shear in the boundary layer near the body and grow by extracting energy from the mean flow into the complex behavior known generally as boundary layer turbulence. The turbulent drag on a body moving in this fluid is primarily due to this excitation of vortex motion, and the subject has properly been of substantial interest for many years. This paper reports on the analysis of data observed on a flow around an axisymmetric test vehicle while it rises under its own buoyancy. This configuration simplifies the flows by making them nearly two dimensional and still exposes flows of significant practical importance. In the study of open flows over flat plates the turbulent region is marked by coherent structures [1,2] which appear partly as horseshoes of localized vorticity bent from lines of spanwise vortices by the mean flow, at least in the part of the boundary layer furthest from the wall, and partly as streamwise vortex structures near the wall. The appearance of these vortices and coherent structures even at high-Reynolds number makes it plausible that only a few degrees of freedom might dominate the boundary layer flow even far downstream from the prow of the test vehicle. In the present case, this idea is well established by the parameters of the flow and the observations about the coherent structures as summarized by Cantwell [1] and Robinson [2]. We return to this connection shortly.

The main result of the analysis in this paper is that methods which identify the nonlinear dynamical degrees of freedom directly in time domain reveal that in this experiment a small number of degrees of freedom are sensed by the pressure sensors flush mounted on the body to view pressure fluctuations in the boundary layer. While we shall have more to say about the boundary layer fluctuations, the fact that the sensors reveal only a few degrees of freedom to be active is consistent with having

*Also at: Institute for Nonlinear Science, University of California, San Diego, La Jolla, CA 92093.

the many degrees of freedom not residing in coherent or larger scale motions significantly damped out in the observed regime of fluid flow. While small scale motions are present at some amplitude, they are "in the noise" relative to the observed degrees of freedom, and we would neither expect to see them nor expect to have them play any significant role in the dominant dynamics of the phenomena seen by the sensors. This runs contrary to the idea that an enormous number of degrees are active in high-Reynolds-number flows. However, it is to be considered an aspect of the degrees of freedom that the sensors used in this experiment can actually sense with distinguishable amplitude. We shall argue that the mathematical idea that the dimension of the flow is enormous is not contradicted by the fact that real world sensors can be influenced by only a subset of those degrees of freedom. This idea calls for the introduction of additional grounds for reasoning about the dimension of an observed time series, going beyond the strict guidelines of the time delay embedding results [3–5] or the direct determination of dimension or active degrees of freedom from numerical simulations [6] which contain no consideration of the properties of the sensors involved in the observations.

A. Description of the experiment

The experiment was conducted in a deep fresh water lake (Lake Pend Orielle) at a facility operated by the David Taylor Research Center/Acoustic Research Detachment in Bayview, Idaho. A buoyant test vehicle was used for the experiment. The test vehicle was propelled vertically from a depth of 1100 ft near the bottom of the lake by its own buoyancy. See Fig. 1 for a representation of the experimental setup. The vehicle was an axisymmetric body 21 in. in diameter and approximately 27 ft in length. Included in the body was a weight section which held a symmetrically distributed array of cylindrical lead weights. Depending on the weight in this section, vehicle speeds of 40 to 75 ft/sec (12.2 m/sec to 22.9 m/sec) were attained. In the experiment analyzed here the speed was 70 ft/sec (22.9 m/sec).

The nose of the test vehicle (see Fig. 2) was instrumented with piezoelectric pressure transducers arrayed along the axis of the text body to measure the pressure fluctuations associated with the developing boundary layer and the resulting turbulence. The transducers were PCB Model 112M149 having a sensitivity of 50 mV/psi (−26 dB/1 V/psi). The physical diameter of the transducers was 0.218 in. (0.55 cm), and the effective diameter over which the instrument was sensitive to the flow, based on a rolloff of −6 dB, was found to be 0.12 in. (0.30 cm) [7]. The pressure transducers were mounted in a carbon-graphite nose shell with stainless steel inserts as shown in Fig. 3. The entire shell surface was covered with an 0.125 in. (0.32 cm) elastomer in order to provide a smooth surface over which the boundary layer could develop. In this configuration the transducers did not trip the flow by form drag. In effect, they were flush mounted because of the elastomer covering.

The vehicle was hauled down to a depth of 1100 ft (335.5 m) via a cable attached to an onshore winch. Once the vehicle was stopped at the bottom of the lake, the onboard Honeywell 5600C tape recorder was powered on and ambient data from all sensors were recorded for 30 sec. Following the ambient recording, the vehicle released itself from the cable and ascended under its own buoyancy towards the lake surface. For a vehicle speed of 70 ft/sec, steady state conditions were achieved at a depth of 700 ft (213.5 m). At 160 ft (48.8 m) the vehicle spread "fins" which turned the vehicle horizontal so the surface would not be broached and result in damage to the electronics. The data reported on in this paper were taken during a 5-sec interval of the steady part of the experimental run while the vehicle was between 550 and 200 ft below the surface.

The Fourier spectra of pressure fluctuations measured by transducers in laminar, transitional, and turbulent flow regimes are shown in Figs. 4–8. The length Reynolds number and displacement thickness δ are also shown in the figures. δ was computed using the Transitional Analysis Program System (TAPS) [8]. Because there are no measurable pressure fluctuations in laminar flow, the Fourier spectrum in that region consists of transducer response to the fluid loaded nose vibration and not to boundary layer pressure fluctuations. This

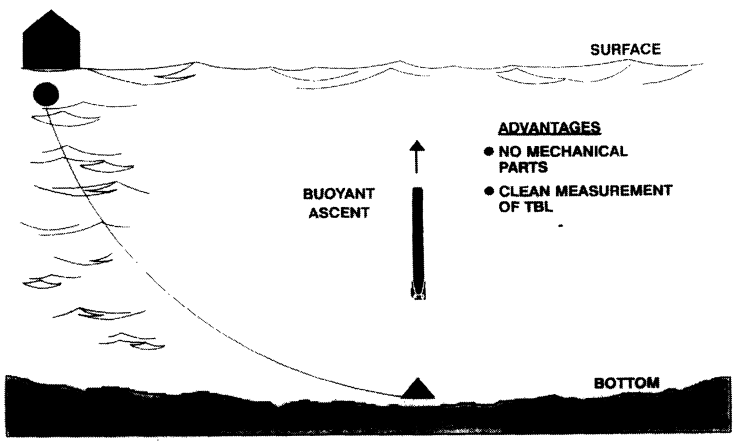

FIG. 1. The setup of the experiment on the buoyant test vehicle. The vehicle was launched at ≈300 m depth and rose freely to about 50 m, where it turned to avoid breaching the surface. Data were taken every 15.26 μsec for 5 sec while the vehicle was in free flight.

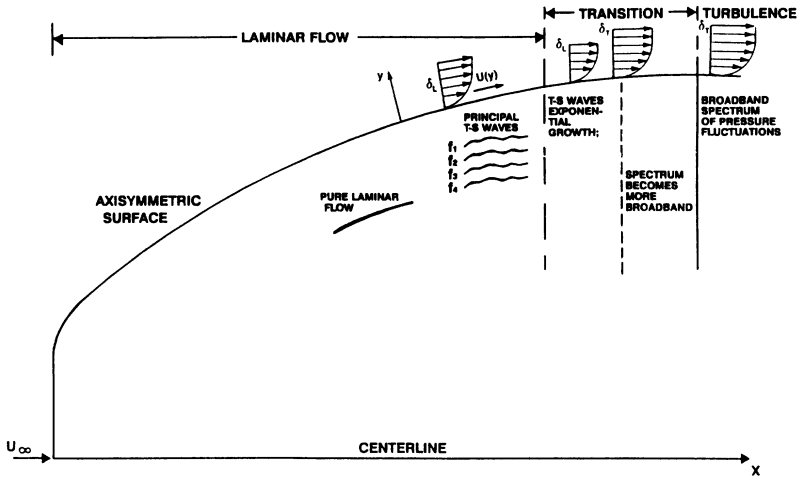

FIG. 2. Schematic of the nose of the test vehicle showing the laminar, transition, and turbulent regions. Below the region designations is an indication of the physical processes dominant in that region. The vehicle was axisymmetric, so the designations hold around the body.

will be clear in all of our later analysis as well, and it is important to keep this in mind as we proceed below. Transition and turbulent data are dominated by boundary layer fluctuations up to 3 or 4 kHz. Further discussion of the experimental situation can be found in [9].

The boundary layer is about $\delta \approx 0.5$ cm. thick (momentum thickness), ranging from 0.16 to 0.6 cm. through the region of the pressure sensors. Using a nominal speed of the vehicle of $u \approx 20$ m/sec, we deduce a typical turnover time or inverse shear in the boundary layer of $\delta/u \approx 250$ μsec. The importance of the outer flow variables in the behavior of the pressure fluctuations seen on the wall in boundary layer flows is emphasized by the results of Farabee and Casarella [10]. Also, the scaling of vorticity variations, clearly the dominant feature in the boundary layer coherent structures, is much cleaner when done with outer variables [11]. The Reynolds number $u\delta/\nu$ based on these dimensions is about 10^5. The sampling time of $\tau_s = 15.26$ μsec chosen for the acquisition of the data guarantees we will capture the main variations in the pressure due to fluid motions, and the shear rate of ≈ 4 kHz means we will lose little by the low pass filtering done at 6400 kHz.

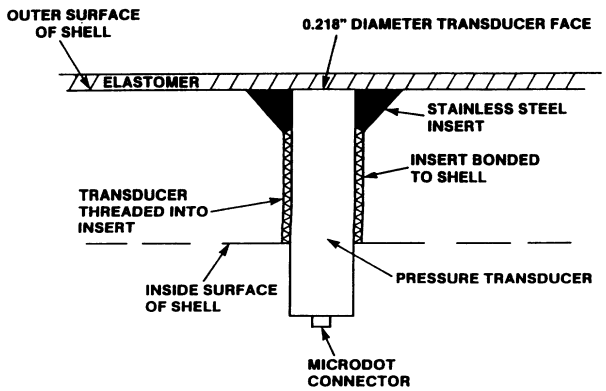

FIG. 3. Configuration of the pressure sensors.

B. Tools used in analysis of the experiment

We have performed analysis of numerous data sets from these experiments using 4 to 5 sec of data in each set. This results in 262 144 points for 4 sec of data and 327 680 points for 5 sec of data. The tools we have used to examine the data include the familiar examination of the time traces and the Fourier spectrum of these. We will show that these tools reveal useful but limited information about the dynamics. We have also studied characteristics of the nonlinear motion [5,12] with:

(i) *Average mutual information,* which determines the way in which measurements at time t nonlinearly correlate [13] with measurements at time $t' \neq t$. We will show that the typical information decorrelation time in the *transition and turbulent* regions is about $15\tau_s \approx 230$ μsec. This is consistent with the fluid dynamical time scales associated with the inverse shear estimated above.

(ii) *Global false nearest neighbors,* which determine in what dimension the attractor in this fluid flow is unfolded [14] in a coordinate system composed of time lags of the pressure measurements taken at lags determined by the average mutual information.

(iii) *Local false nearest neighbors,* which tell us the dimensions of the dynamical model to be used to describe the data [15].

We began the evaluation of the local and global Lyapunov exponents for these attractors [5], but even with the very large data sets we did not convince ourselves that we have sufficient data for the accurate evaluation of these important quantities. We are continuing work on these as they dictate the predictability of the data we are observing. The issue has to do with the evaluation of these exponents in dimensions as high as 8–10. We did conclude that in the transition region where the dimension is lower at least one exponent is positive, consistent with the idea of low dimensional chaos, and has a value about $(10\tau_s)^{-1}$. One exponent is always zero which tells us that the dynamics is governed by a set of differential equations. We shall return to these important questions in a subsequent article.

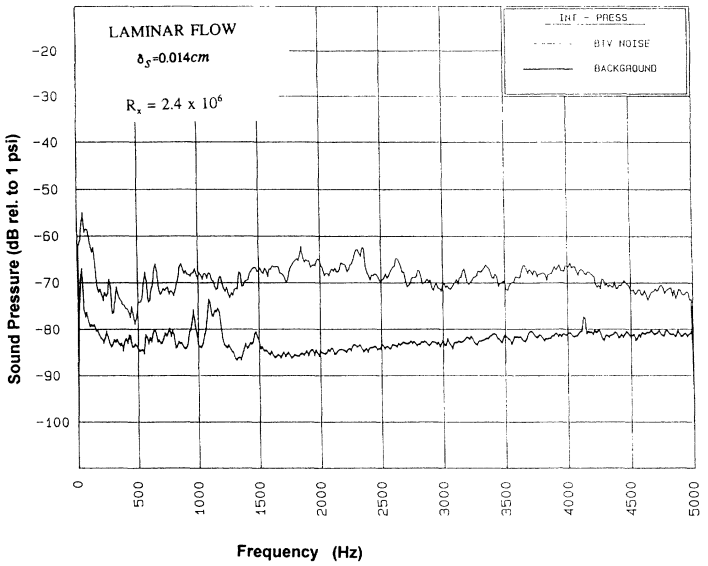

FIG. 4. Fourier power spectrum of the time series for sensor $B1$ located in the laminar zone of the flow. Spectra are shown for the ambient pressure when the vehicle was at rest (this is the heavy solid line designated as BACKGROUND) and for flow conditions as described in the text (light solid line).

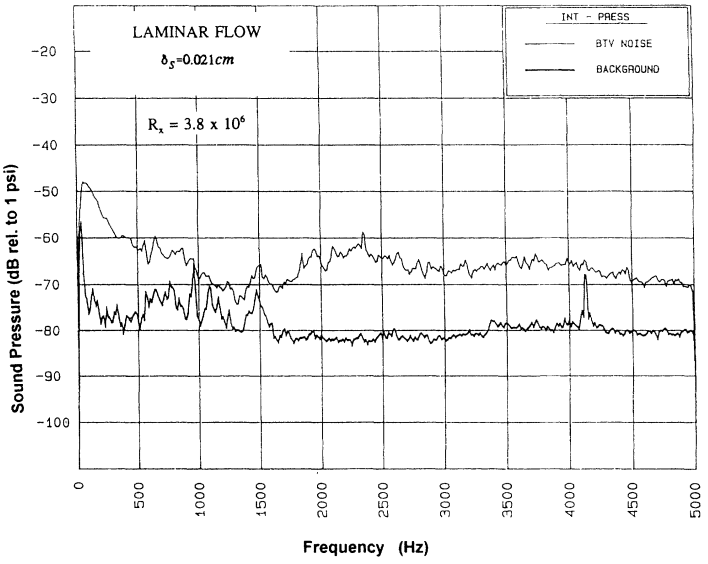

FIG. 5. Fourier power spectrum of the time series for sensor $B3$ located in the laminar zone of the flow. Spectra are shown for the ambient pressure when the vehicle was at rest (this is the heavy solid line designated as BACKGROUND) and for flow conditions as described in the text (light solid line).

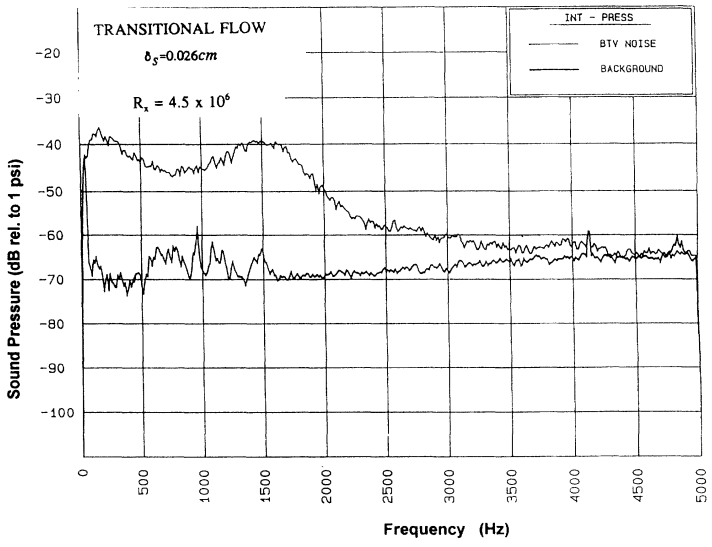

FIG. 6. Fourier power spectrum of the time series for sensor $B4$ located in the transition zone of the flow. Spectra are shown for the ambient pressure when the vehicle was at rest (this is the heavy solid line designated as BACKGROUND) and for flow conditions as described in the text (light solid line).

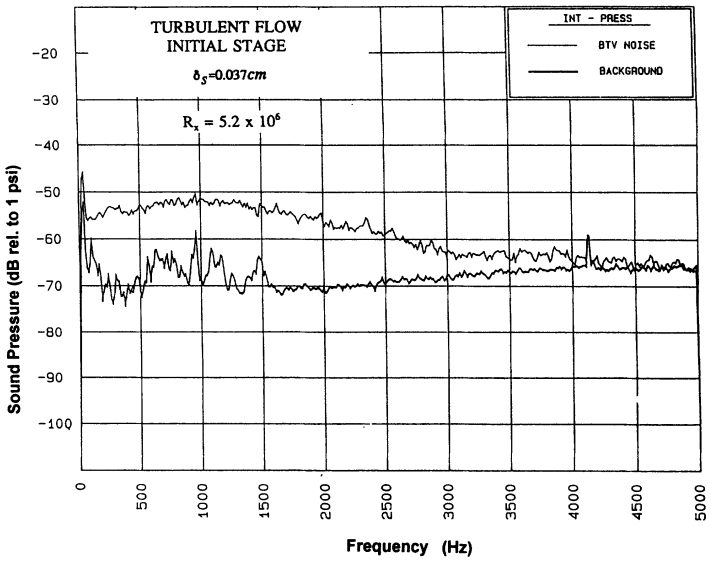

FIG. 7. Fourier power spectrum of the time series for sensor $B5$ located in the turbulent zone of the flow. Spectra are shown for the ambient pressure when the vehicle was at rest (this is the heavy solid line designated as BACKGROUND) and for flow conditions as described in the text (light solid line).

C. Scales in the experiment

In the Cantwell and Robinson review articles [1,2] we find the introduction of "wall units" to be an enormously useful way to capture qualitatively the scales of any given experiment. These units are defined in terms of the stress τ_w at the wall which in turn defines a friction velocity u_τ,

$$u_\tau = \left[\frac{\tau_w}{\rho} \right]^{1/2} , \tag{1}$$

where ρ is the density of the fluid. From this velocity and the kinematic viscosity ν of the fluid, a length scale,

$$\frac{\nu}{u_\tau} , \tag{2}$$

is introduced. In the present experiment we establish a feel for the size of things by using the values for these quantities at the location of the sensor $B7$ (location to be given below), where ambient data as well as pressure fluctuations during buoyant rise of the body was made available for analysis. Using the value $\nu = 1.57 \times 10^{-2}$ cm^2/sec for water and the value $u_\tau = 72.8$ cm/sec deduced from the experimental setup and the program TAPS [8], we find a length scale for wall units of 2.16×10^{-4} cm. In these units the effective sensor size is about 1400 wall units.

The distance between streamwise coherent structures in the turbulent boundary layer has been observed to be about 100 wall units. Similarly, the size of a horseshoe or hairpin structure is around 150 to 200 wall units. With these estimates we see that on the order of ten coherent structures would be within the sensitivity area of the sensors used in the experiment. On these grounds, we would expect that the dynamics of these few coherent structures should totally dominate the observations here. This is further supported by the observations of Schewe [16], who analyzed the ability of pressure sensors on the wall

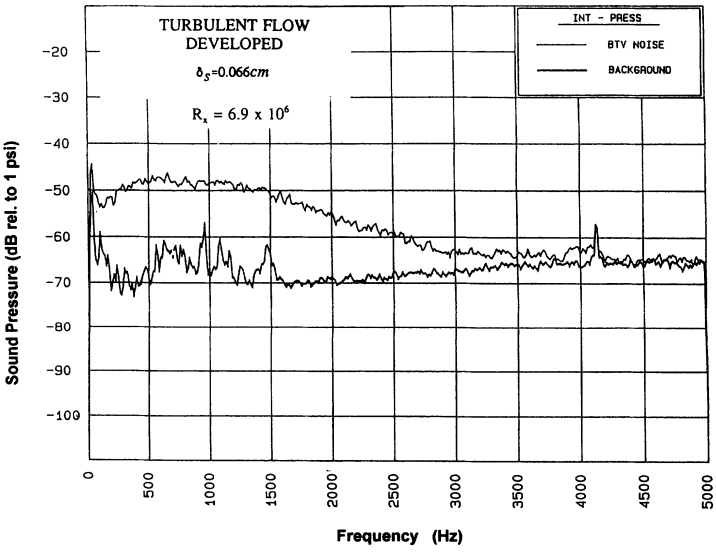

FIG. 8. Fourier power spectrum of the time series for sensor $B7$ located in the turbulent zone of the flow. Spectra are shown for the ambient pressure when the vehicle was at rest (this is the heavy solid line designated as BACKGROUND) and for flow conditions as described in the text (light solid line).

to identify all degrees of freedom in a turbulent boundary layer flow. He concluded that when the sensor is about 20 wall units or less it picks up the finest details of the flow, but as one increases the sensor size it becomes sensitive to other aspects of the flow. Schewe studied sensor sizes from 19 to 333 wall units in diameter. Our sensors are 70 times bigger than this suggested size of 20 wall units, and it is quite plausible that they average out pressure fluctuations on the smallest scales and report only effects due to the larger scale coherent structures of which we estimate an order of 10 are active in the sensors range.

Finally, our Fourier spectra for the transition and turbulent regions peak in the vicinity of frequencies given by $2\pi f\delta/u_r \approx 50$ to 70, which is just in the region that Farabee and Casarella [10] identify as the signature of the maximum effect of outer flow dynamics on the wall pressure fluctuations. Defining the outer scale frequency by $f_o^{-1}=2\pi\delta/u_r$, we have $f_o \approx 23.2$ Hz. The region $f \leq 5f_o \approx 116$ Hz is called the low frequency regime in [10] and identified as coming from large distances from the wall and contributing less than 1% of the total rms pressure fluctuations. These frequencies were filtered out of the present data in any case. The region $f \approx 50f_o$ is called the midfrequency region in [10], and their analysis quite clearly associates this regime with turbulent activity in the outer region of the boundary layer. This is consistent with the other scale estimates we have made here.

II. DATA ANALYSIS

We will present the analysis of many data sets from the experiments just described. The first group are the stations designated $B1$, $B3$, $B4$, $B5$, and $B7$ along one of the axial lines of sensors arrayed on the buoyant test body. We also look at data from the sensor at $B7$ when the test vehicle was sitting motionless at the lake bottom and at data from the fore mounted accelerometer during motion. The ambient data sets a scale and qualitative description of the "noise" in the system. The accelerometer gives a look at the excitation of the structural modes of the body, and this will be seen in contrast to the fluid fluctuations observed by the pressure sensors. The data sets $B1$ and $B3$ are in the "laminar" regime where pressure fluctuations from the fluid motion should be minimal. Indeed as we emphasized above there should be no fluid dynamical pressure fluctuations in the laminar region, so what we see here are either instrumental fluctuations or pressure associated with fluid-loaded vibrations of the hull of the buoyant body. The data set $B4$ is in the "transition" regime, and the sets $B5$ and $B7$ are in the "turbulent" regime. To assure ourselves that conclusions about one region of flow or another are not specific to the line of "B" sensors, we have also looked at data sets from stations $C2$, $F3$ in the laminar regime, $C4$, $C5$, and $E4$ in the transition regime, and $A8$ and $A7$ in the turbulent regime. We will not display the complete analyses for these stations as the results do not further illustrate the points to be made with the B-station data. Since the results for the transition and turbulent regions are quite striking, we will present material from the analysis of the sensors at stations $C5$ and $A8$. The former is in the transition region and the latter near the end of the sensor chain in the turbulent region. The behavior of the pressure fluctuations from these and all the other stations is entirely consistent with that which is presented from the B stations in the respective regimes.

Chaos is a phenomenon in multivariate state space. It may be observed as a scalar time series as we do here in output voltages from a sensor, but we need to reconstruct a many dimensional phase space for viewing the chaotic structure and for computing distinguishing characteristics of the data. The method we use for this is called time delay state space reconstruction [3–5,12] and consists of making d-dimensional vectors from the time delays of the observations. Thus from measured voltages $v(n) = v(t_0 + n\tau_s)$ we make vectors

$$\mathbf{y}(n)=(v(n),v(n+T),v(n+2T),\ldots,v(n+(d-1)T)) , \tag{3}$$

and the first task is to find T and d.

A. Ambient data

We begin with the data set taken at station $B7$ before the vehicle was launched. This is the ambient data. In Fig. 9 we show the time trace of the voltage measured as the output of the pressure transducer as a function of time. This is about 10% of the recorded data stream. The Fourier power spectrum for this data shows a rather flat spectrum until the roll off at 6400 Hz, due to the low pass filter.

1. Average mutual information

Next we will display the average mutual information calculation for the ambient data. At this juncture we will digress to explain the statistic we are computing so the reader can understand what we are evaluating.

Nonlinear systems in a parameter regime where the orbits are chaotic are known to generate entropy in the direct sense of Shannon [5]. This suggested to several authors [13] that the information theoretic properties of

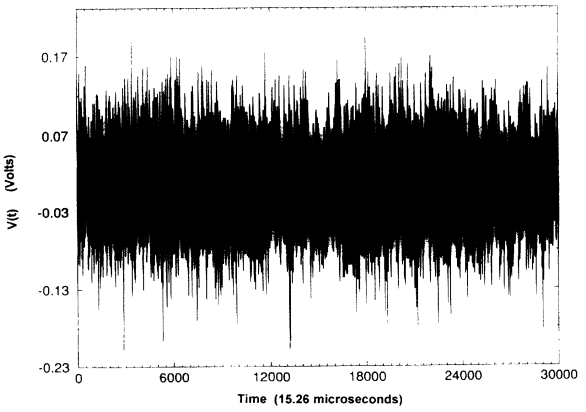

FIG. 9. The time trace of voltage from the pressure transducer at location $B7$ in the ambient state. The vehicle was at rest.

chaotic systems would be particularly useful in their study. The average mutual information is one of those tools. It answers the question: if we have made a measurement of voltage from the pressure sensors $v(n)=v(t_0+n\tau_s)$, how much information (in bits) do we have about the measurement of voltage (pressure) a time $T\tau_s$ later; namely, $v(n+T)$? The information theoretic answer to this question requires the distribution of the measurements $v(n)$ and $v(n+T)$ (the distribution of these is the same) over the set of measured data and the joint distribution of measurements of these two quantities. The first we call $P(v(n))$, the second, $P(v(n+T))$, and the last, $P(v(n),v(n+T))$. The mutual information between these measurements is

$$\log_2\left[\frac{P(v(n),v(n+T))}{P(v(n))P(v(n+T))}\right], \tag{4}$$

and the average over all measurements is

$$I(T)=\sum_{n=1}^{N} P(v(n),v(n+T)) \times\log_2\left[\frac{P(v(n),v(n+T))}{P(v(n))P(v(n+T))}\right], \tag{5}$$

when we have N observations. $I(T)$ is the average mutual information. If the measurements $v(n)$ and $v(n+T)$ are independent, then each term in this sum vanishes since the joint probability factorizes $P(a,b)=P(a)P(b)$. We expect the two measurements to become independent for very large T since chaotic signals rapidly lose memory of earlier entries on their orbits. $I(T=0)$ is large. It reflects the full knowledge we have of the measurements. The actual value, $I(0)$, is the Shannon entropy. In general, $I(T)>0$, and we seek some intermediate value of T where $I(T)$ is not too large or too small. If we can find such a value, then that T will serve as a candidate for determining rather independent measurements $v(n)$ and $v(n+T)$—independent in a nonlinear sense. A nonlinear *prescription*, similar in spirit to the *prescription* often used in linear analysis of choosing the first zero of an autocorrelation function, is to choose the first minimum of $I(T)$. In practice, any time lag in the vicinity of this minimum will do fine, and the mathematical theorem which underlies this construction [3,4] is true, in principle, independent of T.

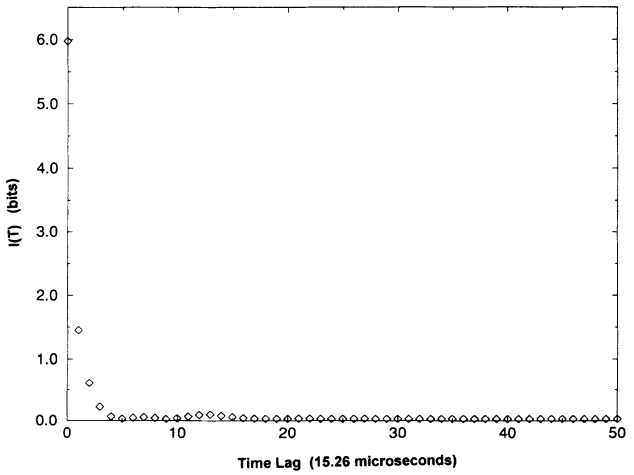

FIG. 10. The average mutual information evaluated from data taken at station $B7$ in the ambient state. The first minimum of $I(T)$ is at $T=5$ or 76 μsec. 327 000 data points were used for this analysis.

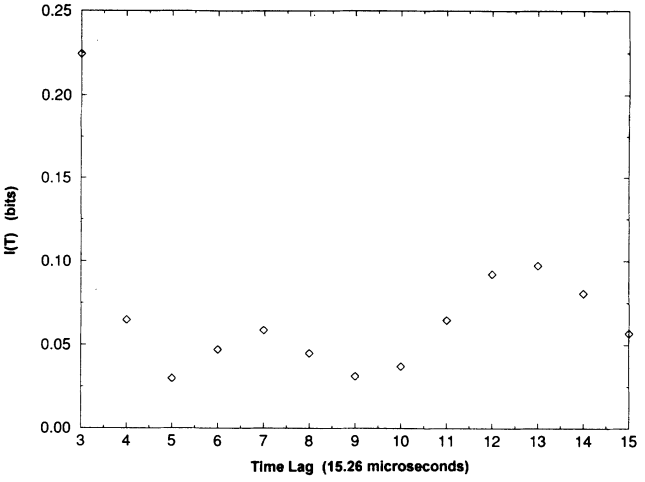

FIG. 11. An expanded scale view of the average mutual information evaluated from data taken at station $B7$ in the ambient state. The first minimum of $I(T)$ is at $T=5$ or 76 μsec. 327 000 data points were used for this analysis.

Evaluating $I(T)$ gives the data shown in Fig. 10. This function has its first minimum at $T=5$ or at a lag of approximately 76 μsec. The region of this minimum is shown in expanded format in Fig. 11. From our earlier comments we would conclude that this delay has little, if anything, to do with time scales associated with the fluid flow.

2. *False nearest neighbors*

To determine an appropriate value for the dimension of the state space in which we will view the observed process, we use a method which inquires into the geometric basis for the theorem of Mañé and Takens [3,4]. The idea is that we observe the data from a multivariate structure projected down onto the observation axis, here, $v(n)$. To unfold this structure we must add additional coordinates for the space. We have added enough additional coordinates when all points are near each other for dynamical reasons rather than because they got there by projection from a higher dimension. We proceed [14] by determining in dimension d which points made out of time delays into vectors as above are the nearest neighbors $\mathbf{y}^{\mathrm{NN}}(n)$,

$$\mathbf{y}^{\mathrm{NN}}(n)=(v^{\mathrm{NN}}(n),v^{\mathrm{NN}}(n+T),\ldots,v^{\mathrm{NN}}(n+(d-1)T)), \tag{6}$$

of the point $\mathbf{y}(n)$. Then we ask whether these points remain near in dimension $d+1$, where the vector $\mathbf{y}(n)$ is augmented by a component $v(n+dT)$ and $\mathbf{y}^{\mathrm{NN}}(n)$ is augmented by $v^{\mathrm{NN}}(n+dT)$. If this distance is small, then the neighbors are true neighbors. If not, then we have

false neighbors which arrived near each other by projection. When the percentage of false nearest neighbors falls to zero, we have unfolded the attractor.

"Noise," which we have come to understand is high dimensional dynamics, will have a large percentage of false nearest neighbors for any low dimension, say up to 20 or so where we typically stop computing. Eventually, as the number of dimensions reaches that of the dynamical rule generating the "random" numbers, the percentage of false nearest neighbors will drop to zero. If we add a high dimensional signal to a low dimensional signal [5,14], then the false neighbors will fall for a while and eventually rise. These qualitative statements are dependent on the number of data, but seem to hold as a descriptive feature of this kind of data.

In Fig. 12 we show the percentage of false nearest neighbors for the ambient data using the time delay of $T=5$ indicated above and using first 17 000 and then 87 000 data points. It is clear from this graph that the ambient data represent a high dimensional signal. Indeed, from this test, with the computing power we presently have and the number of data available, we cannot say in what dimension the data may be unfolded, except to agree that it is higher than 20. In Fig. 13 we show for comparison the false nearest-neighbor computation for the Lorenz model [17], which is composed of three ordinary differential equations. The computation is shown for the clean chaotic signal, the same signal with 50% ($S/N=6$ dB) uniform random noise added, and the same signal with 100% ($S/N=0$ dB) uniform random noise added.

It is clear from this example that the ambient signal may be composed of a low dimensional signal plus some high dimensional noise, but no quantitative test for this kind of conclusion is yet available. The qualitative suggestion, however, arguing by analogy with the behavior

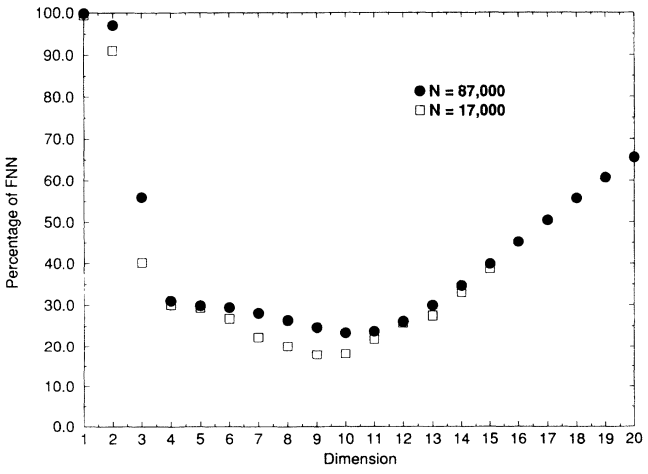

FIG. 12. Global false nearest neighbors for the data from station $B7$ when the vehicle was at rest. The time delay of $T=5$ used in constructing phase space vectors $\mathbf{y}(n)$ is taken from the first minimum of the average mutual information. Results are shown for $N=17\,000$ and $N=87\,000$ data points. The implication that the ambient data is high dimensional is independent of the number of data in this range.

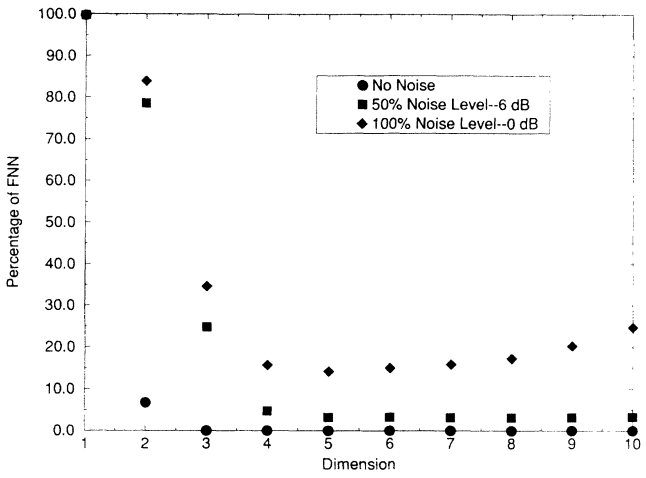

FIG. 13. Global false nearest neighbors for data from one of the components of the three degree of freedom Lorenz model [17]. The false nearest neighbors are shown when the data are clean, when we have added uniform random numbers with an rms level of 50% of the size of the attractor, and when we have added noise at 100% the size of the attractor. The false nearest neighbor calculation degrades gracefully with contamination. This figure suggests that in some of the data analyzed in this paper we may be seeing a low dimensional system contaminated by high dimensional "noise." $T=10$ was used in these calculations.

of the Lorenz data contaminated at various levels is both suggestive and interesting.

The false nearest-neighbor test thus establishes here that this ambient data is noiselike, and we can proceed no further with our analysis of this data using the tools presently available for nonlinear systems. More precisely, when a signal is shown to be high dimensional, the analysis tools for working further with that signal are basically not well developed at this time. The distinction between *low* and *high* dimensional is not one made in principle but in practice and the qualitative break point is about dimension 8 to 10. In any case, we will see quite a different behavior for transition and laminar data. We have presented this in detail since when we come to other test vehicle data sets, the contrast will be striking.

B. Laminar data

Next we examine data, from the laminar region. The time series of voltage from station $B1$ is shown in Fig. 14. It is irregular, appearing much as the ambient data. Note the low level of voltage (the proxy for pressure) fluctuations in this region. This is consistent with the designation laminar, where no pressure fluctuations should occur. In Fig. 15 we have the average mutual information for this data set; zero lag is suppressed. We can clearly see a minimum at $T=7$, or $7\tau_s \approx 107$ μsec. This is similar to the first minimum for the ambient data set, and indicates that the time delay here is characteristic of something other than the fluid flow. Next examine the false nearest neighbors for this data. In Fig. 16 we show this for dimensions $1 \leq d \leq 20$ using 87 000 data points

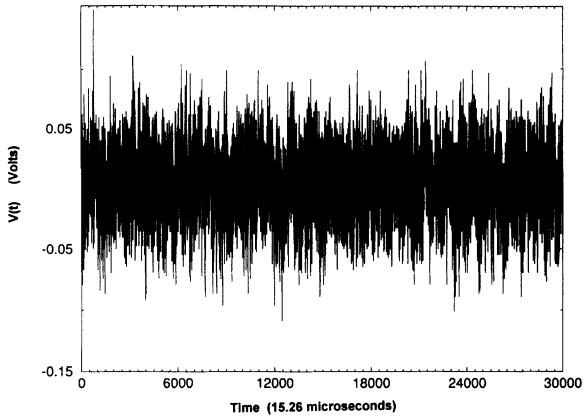

FIG. 14. Time series of voltage from the pressure transdducer located at station $B1$ in the laminar region during the rise of the vehicle. Note the low voltage levels compared to the transition and turbulent regions seen below. In noise free fluid flow there should be no pressure fluctuations in the laminar region.

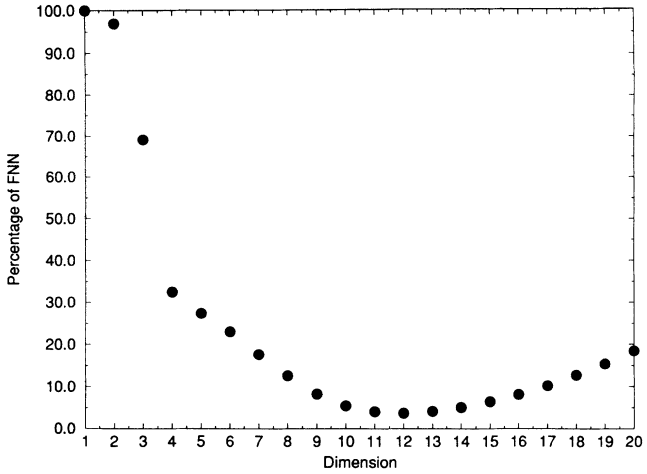

FIG. 16. Global false nearest neighbors for the data from station $B1$ when the vehicle was in motion. The time delay of $T=7$ used in constructing phase space vectors $\mathbf{y}(n)$ is taken from the first minimum of the average mutual information. Results are shown for $N=87\,000$ data points.

from the measurements. Once again we cannot say what dimension should be used for unfolding an attractor for this data, except that it is quite high. One might conclude that there is some evidence that an underlying dynamical process of some low dimension, of order 7 or so, has been seen here contaminated by substantial amounts of noise from other sources. False nearest neighbors is not a fine tuned enough tool to make that kind of conclusion firm.

A similar set of results applies for the data from station $B3$, which is also in the laminar region. Neither the time series nor the power spectrum is very revealing. In Fig. 17 are the results for average mutual information for this data station. There is again a clear minimum at $T=7$, and that is the one we use in reconstructing the vectors in multivariate phase space. In Fig. 18 is the result for false nearest neighbors for this data. We reach the same conclusions just as before for the other laminar flow data.

In a sense this is surprising, and in another sense this is natural. Of course, one expects laminar flow to be regular and low dimensional. Indeed, it is. From the point of view of pressure fluctuations, perfectly clean data should have dimension zero; that is, no pressure fluctuations in laminar flow. However, we have data dominated by the transducer response to fluid-loaded nose vibrations. The indications of this are the levels of the fluctuations, and even more telling is the place where average mutual information has its first minimum (namely $T\approx 5-7$) characteristic of some time scale other than that of the fluid flow. Finally, the false nearest-neighbor test shows that each of the ambient and laminar data sets is very high dimensional.

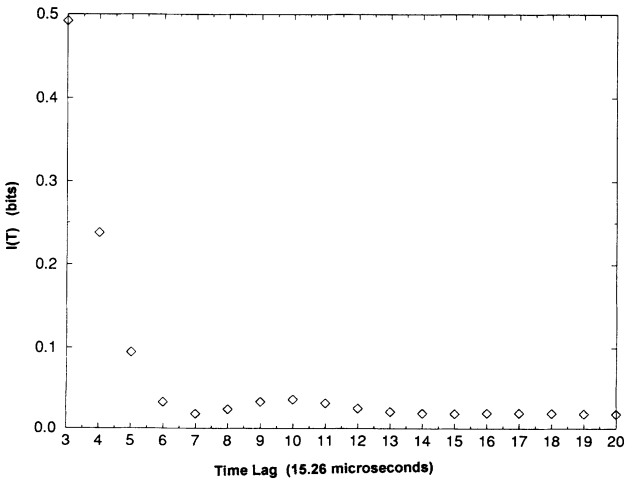

FIG. 15. The average mutual information evaluated from data taken at station $B1$ in the laminar zone during the rise of the vehicle. The first minimum of $I(T)$ is at $T=7$ or 107 μsec. 327 000 data points were used in this calculation.

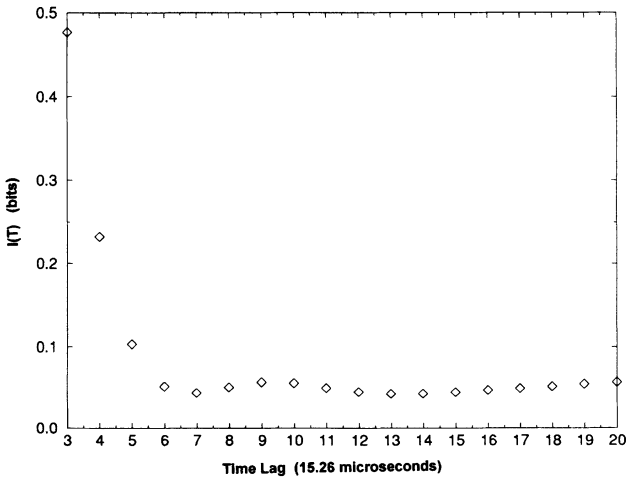

FIG. 17. The average mutual information evaluated from data taken at station $B3$ in the laminar zone during the rise of the vehicle. The first minimum of $I(T)$ is at $T=7$ or 107 μsec. 327 000 data points were used in this calculation.

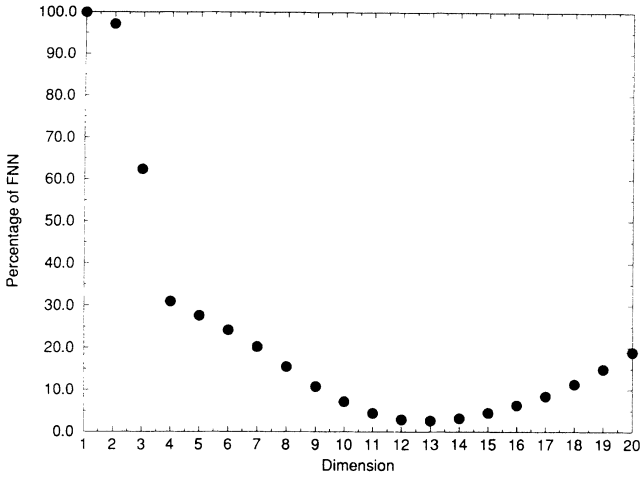

FIG. 18. Global false nearest neighbors for the data from station $B3$ when the vehicle was in motion. The time delay of $T=7$ used in constructing phase space vectors $\mathbf{y}(n)$ is taken from the first minimum of the average mutual information. Results are shown for $N=97\,000$ data points.

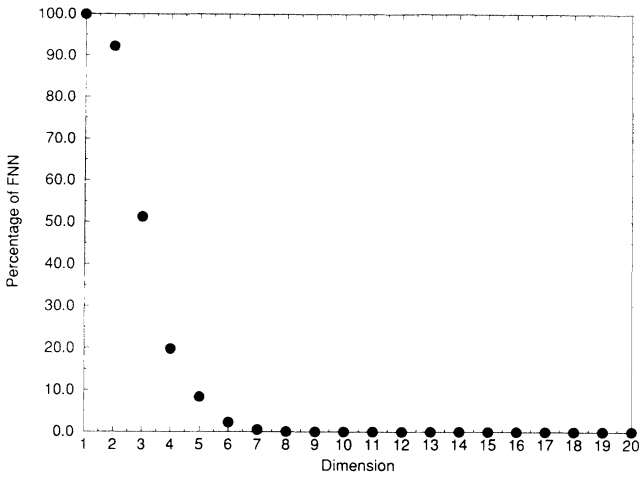

FIG. 20. Global false nearest neighbors for the data from station $B4$ when the vehicle was in motion. The time delay of $T=16$ used in constructing phase space vectors $\mathbf{y}(n)$ is taken from the first minimum of the average mutual information. Results are shown for $N=97\,000$ data points. The fall of false nearest neighbors to zero at dimension 7 is a result of low dimensional dynamics as the source of the pressure fluctuations.

C. "Transition" region data

Now we come to much more interesting data. In the transition region we should see some evidence of the production of TS waves, and see some significant pressure fluctuations. The data is now from station $B4$. In Fig. 19 we display the average mutual information which has its first minimum at $T=16$ or about 244 μsec, which is now characteristic of the fluid flow according to our earlier estimates. In Fig. 20 we show the plot of false nearest neighbors for this data for $1 \leq d \leq 20$. This is substantially different from the behavior of earlier data sets. Here the percentage of false nearest neighbors drops to zero at $d=7$ and then remains there. This behavior is characteristic of a low dimensional chaotic system whose attractor has been unfolded at dimension 7.

Since this is so different from the previous data sets, even though the time series and power spectra are not that different, we take a look at another data set from the transition region. The set we chose was from station $C5$, which is located very near the end of the transition region. In the power spectrum for this sensor the region around 1500 Hz where TS waves were located before is

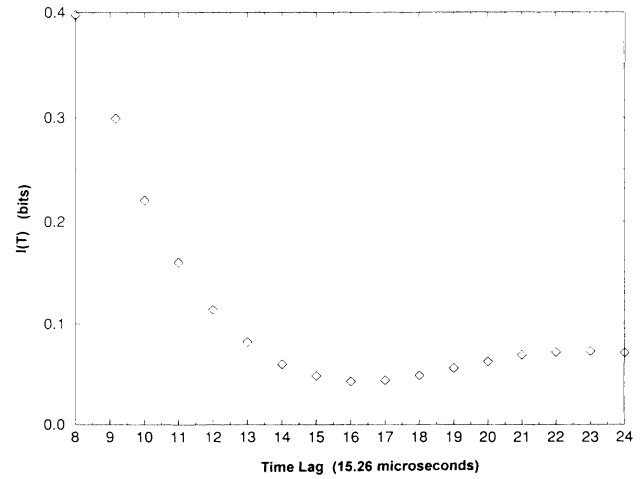

FIG. 19. The average mutual information evaluated from data taken at station $B4$ in the transition zone during the rise of the vehicle. The first minimum of $I(T)$ is at $T=16$ or 244 μsec. This is a time scale consistent with the fluid dynamics of the boundary layer. 327 000 data points were used in this calculation.

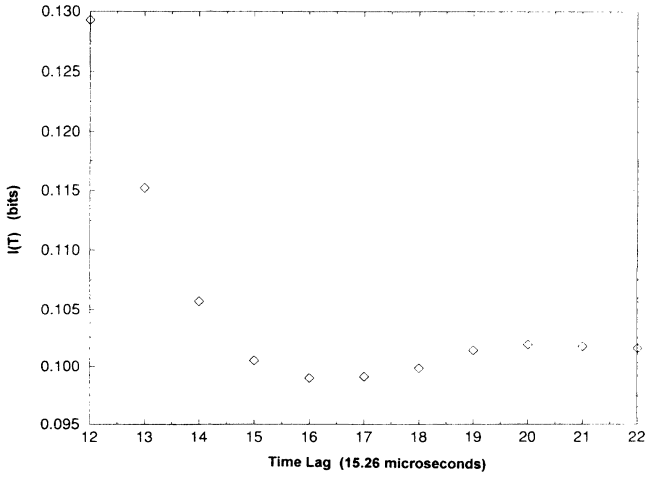

FIG. 21. The average mutual information evaluated from data taken at station $C5$ in the transition zone during the rise of the vehicle. The first minimum of $I(T)$ is at $T=16$ or 244 μsec. This is a time scale consistent with the fluid dynamics of the boundary layer. 327 000 data points were used in this calculation.

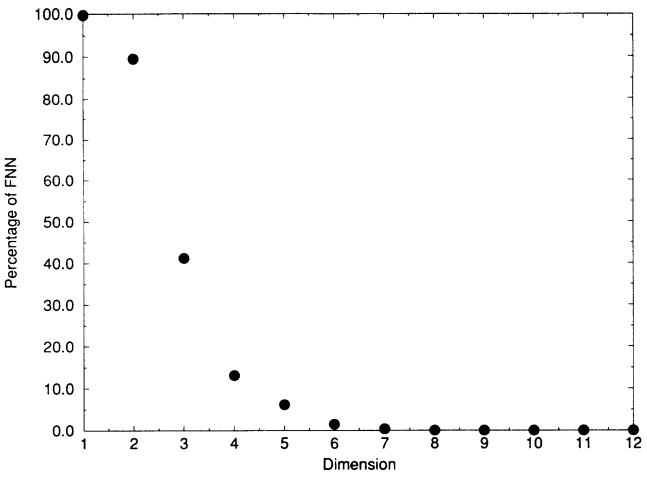

FIG. 22. Global false nearest neighbors for the data from station $C5$ when the vehicle was in motion. The time delay of $T=16$ used in constructing phase space vectors $\mathbf{y}(n)$ is taken from the first minimum of the average mutual information. Results are shown for $N=57\,000$ data points. The fall of false nearest neighbors to zero at dimension seven is a result of low dimensional dynamics as the source of the pressure fluctuations.

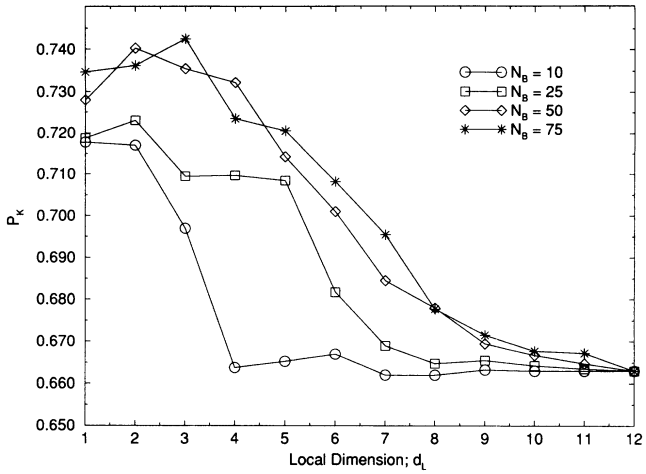

FIG. 23. Local false nearest neighbors for the data from station $C5$ in the transition zone. The time delay $T=16$ comes from average mutual information. $N=65\,000$ data points were used. $\beta=0.54$ measures the fraction of the attractor over which a bad prediction must occur in the local false nearest neighbor calculation. The percentage of bad predictions becomes independent of the number of neighbors N_B and the local dimension near $d_L=9$. $N_B=10$, 25, 50, and 75 were used here.

less distinct, but then we are further down the body than at $B4$ so we have entered a region of more pronounced nonlinear interaction among the modes. The average mutual information for the $C5$ data set is shown for lags $12\leq T\leq 22$ in Fig. 21 where the minimum, the first in this data, is seen at $T=16$. This is the same as in the previous transition data set. In Fig. 22 the false nearest neighbors for this data set is shown for $1\leq d\leq 12$. The false nearest neighbors has dropped below 0.5% at $d=7$ indicating that we almost certainly have unfolded the attractor, though the cautious person would wish to choose $d=8$. In a moment we will provide further evidence that $d=8$ is appropriate. In any case, we see a clear statement that the number of dimensions required to capture this data set, as in the case of station $B4$, is small, namely about 7 or 8. This is in sharp contrast to the laminar or ambient data. Further underlining this as a dynamical feature is the distinguishably higher level of pressure fluctuations seen in the time series and the fluid dynamical relevance of the time delay $T=16$ in units of τ_s.

1. *Local false nearest neighbors*

As another tool for examining the data here, we look at a quantity which asks how many dynamical degrees of freedom are excited locally on the attractor. The global false nearest-neighbor criterion produces a global number, which allows the unfolding of the attractor in the time delay coordinate system. However, since the time delay coordinates are almost certainly not the original coordinates in which the system evolves, it is quite plausible that the embedding dimension associated with the global false nearest neighbors is larger than that of the dynamics itself. To examine this we have created a local false nearest-neighbor test [15], which examines in every neighborhood on the attractor how well one can predict ahead the evolution of two neighboring points in dimensions less than or equal to the dimension given by the global false nearest-neighbor test. If the percentage of bad predictions that may be due to numerical accuracy or the quality of the particular prediction method used becomes independent of local dimension, then that dimension is picked out as the dimension of the dynamics. The basic idea is that when neighbors are false they are nearby for geometric, not dynamical reasons, so they will lead to bad predictions because they will evolve rapidly to far separated parts of the attractor. True neighbors will move along with each other and the quality of one's ability to predict where they will go is not limited by their having been projected together from a higher dimension where they are in fact quite well separated. In Fig. 23 we show the percentage of bad predictions for data set $C5$ as a function of local dimension and of number of neighbors. This shows that at $d=8$, which is the same dimension as the global false neighbor test indicated, the predictability becomes independent of these variables, thus indicating that dimension 8 is correct for this set of observations.

D. Turbulent data sets

Now we examine data from two turbulent data sets. The first is station $B5$, which is located at the beginning of the turbulent region. In Fig. 24 the average mutual information is shown from $5\leq T\leq 22$ and a clear minimum at $T=16$ is revealed. $T=16$ is a time of 244 μsec, which is consistent with fluid flow dynamics. The amplitude of the pressure fluctuations, compared to the ambient or laminar data, supports this conclusion. In Fig. 25 we

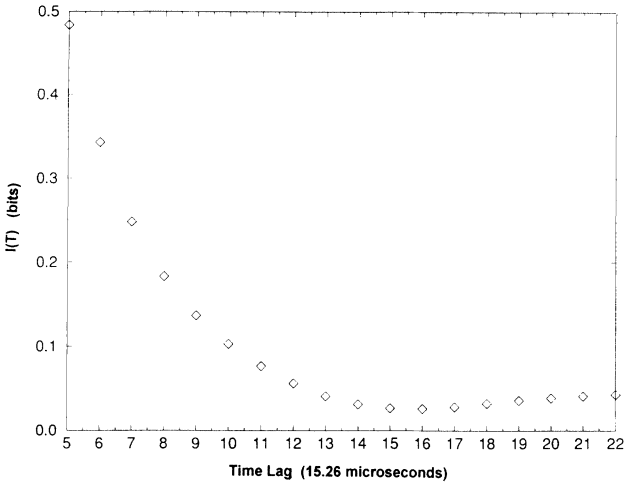

FIG. 24. The average mutual information evaluated from data taken at station $B5$ in the turbulent zone during the rise of the vehicle. The first minimum of $I(T)$ is at $T=16$ or 244 μsec. This is a time scale consistent with the fluid dynamics of the boundary layer. 327 000 data points were used in this calculation.

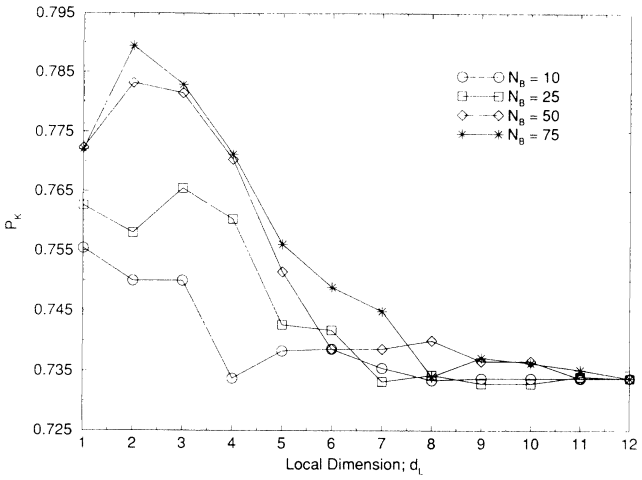

FIG. 26. Local false nearest neighbors for data from station $B5$ in the turbulent zone. The time delay $T=16$ comes from average mutual information. $N=75\,000$ data points were used. $\beta=0.54$ measures the fraction of the attractor over which a bad prediction must occur in the local false nearest neighbor calculation. The percentage of bad predictions becomes independent of the number of neighbors N_B and the local dimension near $d_L=9$. $N_B=10$, 25, 50, and 75 were used here.

have the global false nearest-neighbors result for station $B5$. It is clear that at dimension 9 or 10 we have unfolded the attractor completely. We further examine this conclusion by looking in Fig. 26 at the *local* false nearest neighbors for data set $B5$. Here it is clear that at local dimension 9 we have achieved the independence of local dimension and number of neighbors, which is characteristic of having unfolded the attractor locally.

Our next example is data from station $B7$ located in fully developed turbulent flow. There are no surprises in the time series or the Fourier power spectrum. Figure 27 shows the average mutual information from $10 \le T \le 25$, and the minimum at $T=18$ (the first minimum) is evident. Using this value of the timelag we evaluate the global false nearest neighbors which is shown in Fig. 28; a global embedding dimension of $d=8$ is revealed for this data. In Fig. 29 we display the local false nearest-neighbor calculation for data set $B7$. This makes it quite clear that at dimension 8 we have locally unfolded the attractor and confirms the evidence from the global examination of this question.

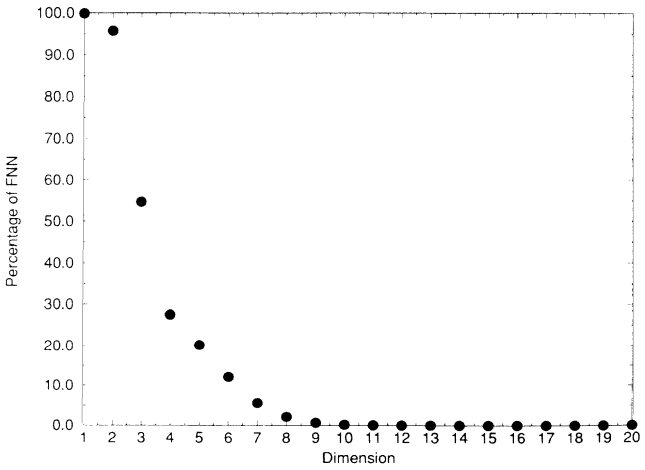

FIG. 25. Global false nearest neighbors for the data from station $B5$ when the vehicle was in motion. The time delay of $T=16$ used in constructing phase space vectors $\mathbf{y}(n)$ is taken from the first minimum of the average mutual information. Results are shown for $N=97\,000$ data points. The fall of false nearest neighbors to zero at dimension 9 is a result of low dimensional dynamics as the source of the pressure fluctuations.

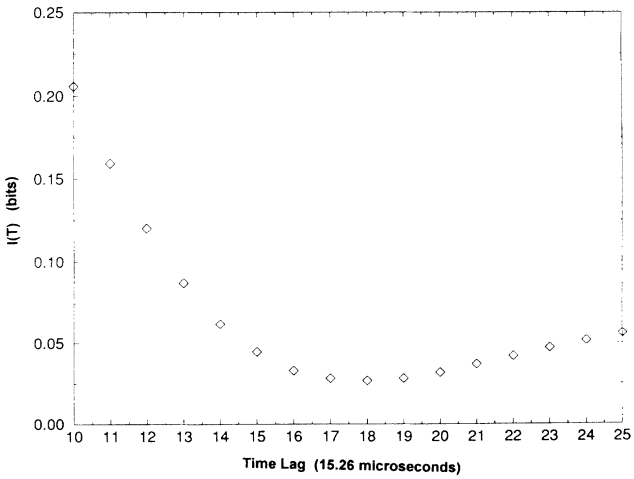

FIG. 27. The average mutual information evaluated from data taken at station $B7$ in the turbulent zone during the rise of the vehicle. The first minimum of $I(T)$ is at $T=18$ or 275 μsec. This is a time scale consistent with the fluid dynamics of the boundary layer. 327 000 data points were used in this calculation.

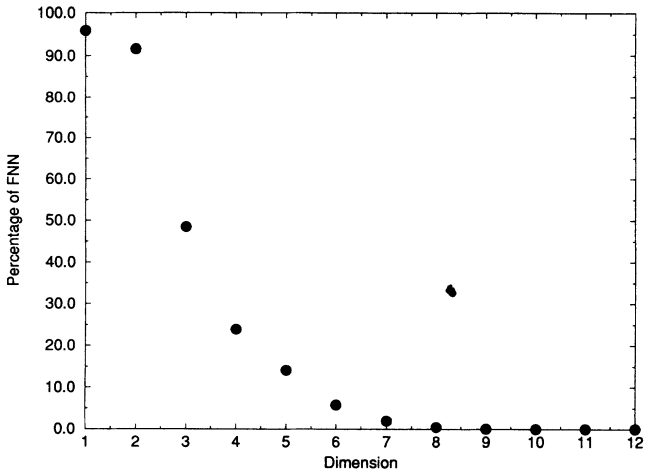

FIG. 28. Global false nearest neighbors for the data from station $B7$ when the vehicle was in motion. The time delay of $T=18$ used in constructing phase space vectors $\mathbf{y}(n)$ is taken from the first minimum of the average mutual information. Results are shown for $N=59\,500$ data points. The fall of false nearest neighbors to zero at dimension 8 is a result of low dimensional dynamics as the source of the pressure fluctuations.

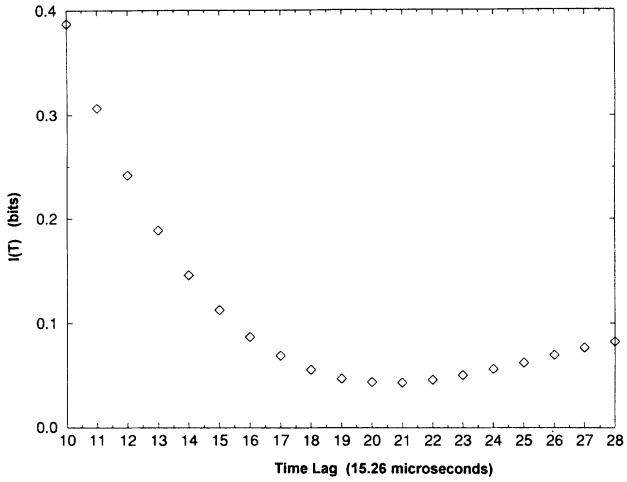

FIG. 30. The average mutual information evaluated from data taken at station $A8$ in the turbulent zone during the rise of the vehicle. The first minimum of $I(T)$ is at $T=20$ or 305 μsec. This is a time scale consistent with the fluid dynamics of the boundary layer. 327 000 data points were used in this calculation.

The last look at data from pressure sensors comes from examining data from station $A8$, which is within the fully turbulent region. In Fig. 30 we show the average mutual information from this sensor. This reveals a clear minimum at $T=20$ corresponding to a timelag of 300.5 μ sec, which is associated with the fluid flow. Using this value of T we determine the percentage of global false nearest neighbors shown in Fig. 31. The percentage drops very near zero by dimension 7, and we zoom in on this data in Fig. 32 where global false nearest neighbors is shown for $6 \leq d \leq 15$ and we see the percentage of false neighbors go to zero at $d=9$ and then stay there. The local false nearest-neighbors test displayed in Fig. 33 confirms that at dimension 9 we have removed all ambiguities in true neighbors by unfolding the attractor.

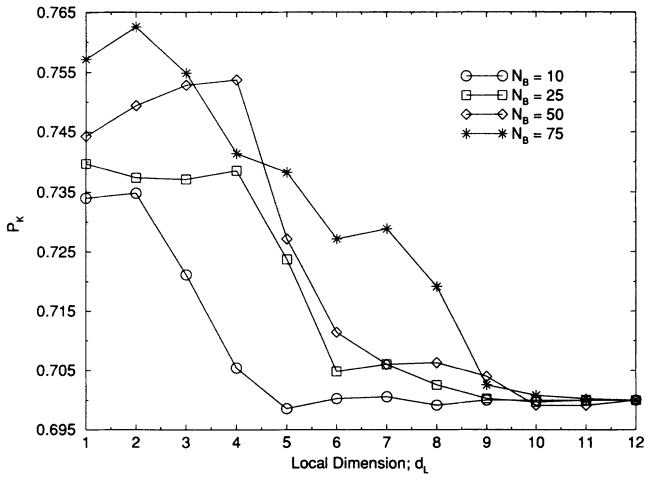

FIG. 29. Local false nearest neighbors for data from station $B7$ in the turbulent zone. The time delay $T=18$ comes from average mutual information. $N=75\,000$ data points were used. $\beta=0.54$ measured the fraction of the attractor over which a bad prediction must occur in the local false nearest neighbor calculation. The percentage of bad predictions becomes independent of the number of neighbors N_B and the local dimension near $d_L=9$. $N_B=10$, 25, 50 and 75 were used here.

E. Accelerometer data

We have one other glimpse of the dynamics in this experiment, namely data from an accelerometer mounted forward in the test vehicle. Using this data we display the average mutual information in Fig. 34 for $3 \leq T \leq 20$;

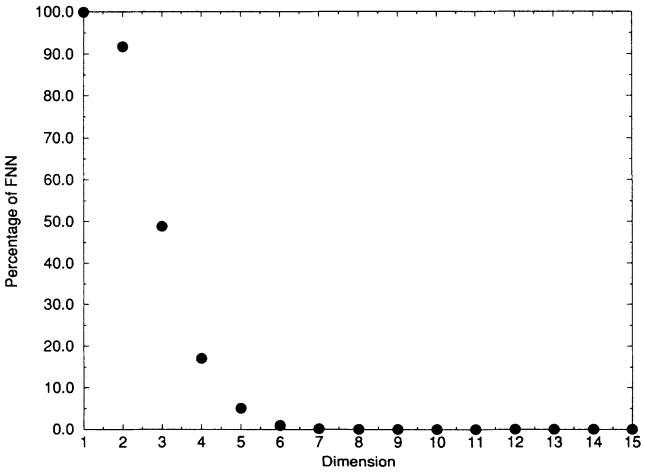

FIG. 31. Global false nearest neighbors for the data from station $A8$ when the vehicle was in motion. The time delay of $T=20$ used in constructing phase space vectors $\mathbf{y}(n)$ is taken from the first minimum of the average mutual information. Results are shown for $N=87\,000$ data points. The fall of false nearest neighbors to zero at dimension 7 is a result of low dimensional dynamics as the source of the pressure fluctuations.

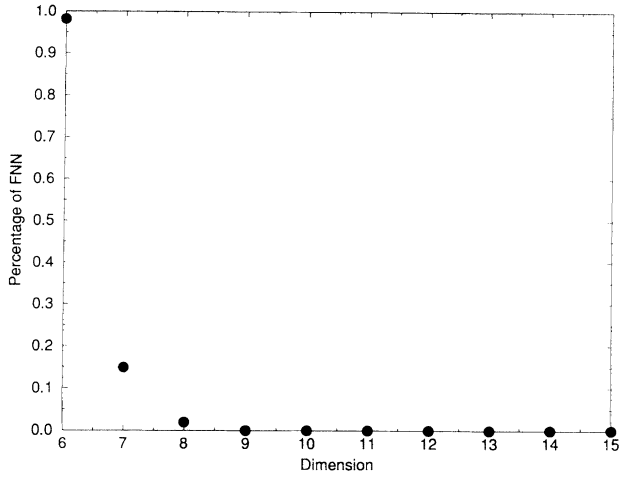

FIG. 32. Expanded scale for global false nearest neighbors for the data from station $A8$ when the vehicle was in motion. $6 \leq d \leq 15$. The time delay of $T=20$ used in constructing phase space vectors $\mathbf{y}(n)$ is taken from the first minimum of the average mutual information. Results are shown for $N=87\,000$ data points.

we see the first minimum of the average mutual information at $T=5$, which does not correspond to fluid dynamical time scales. Finally, using this data we show in Fig. 35 the global false nearest neighbors, which demonstrates that this is very high dimensional dynamics and significantly different from the dynamics of the fluid flow seen in the transitional and turbulent data sets. The accelerometer data is consistent with the laminar data, which represents the response of the transducer to nose vibration.

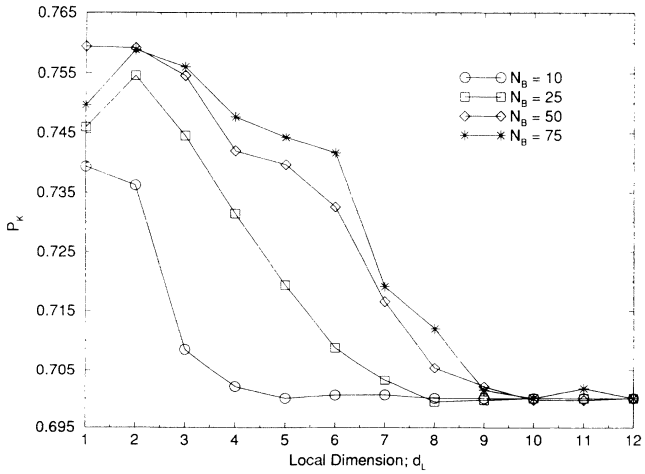

FIG. 33. Local false nearest neighbors for data from station $A8$ in the turbulent zone. The time delay $T=20$ comes from average mutual information. $N=65\,000$ data points were used. $\beta=0.54$ measured the fraction of the attractor over which a bad prediction must occur in the local false nearest neighbor calculation. The percentage of bad predictions becomes independent of the number of neighbors N_B and the local dimension near $d_L=9$. $N_B=10$, 25, 50, and 75 were used here.

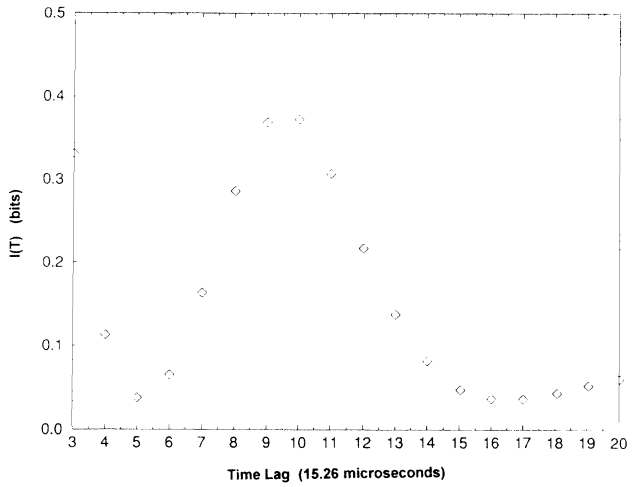

FIG. 34. The average mutual information evaluated from data taken at the forward mounted accelerometer during vehicle motion. The first minimum of $I(T)$ is at $T=5$ or 76 μsec. 262 000 data points were used in this calculation.

III. SUMMARY, CONCLUSIONS, AND FUTURE DIRECTIONS

This paper has analyzed in some detail the pressure fluctuations measured on an axisymmetric body propelled under its own buoyancy at velocities on the order of 20 m/sec. At these velocities and with the momentum thickness of the boundary layer about 0.5 cm, one establishes that the thickness Reynolds number is about 100 000. In such flows there is substantial activity in the form of coherent structure [1,2] whose size in "wall length" units is about 100 wall units spanwise in the lower boundary layer and 150 to 200 units streamwise in the upper boundary layer.

These coherent structures are known to contribute in a

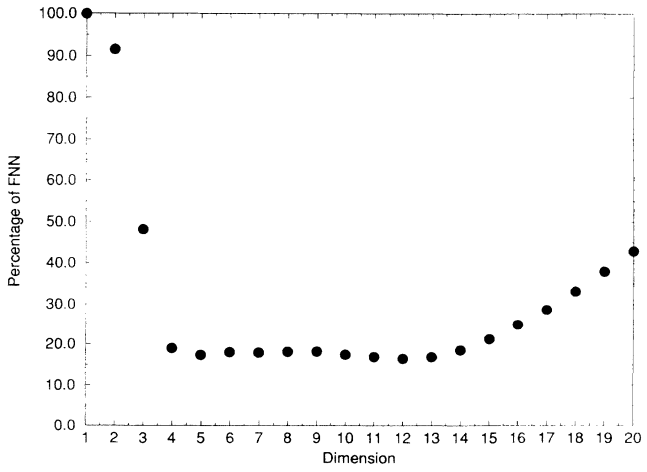

FIG. 35. Global false nearest neighbors for the data from the forward mounted accelerometer when the vehicle was in motion. The time delay of $T=5$ used in constructing phase space vectors $\mathbf{y}(n)$ is taken from the first minimum of the average mutual information. Results are shown for $N=87\,000$ data points.

significant way to the wall pressure fluctuations. The sensors used in this experiment have an effective sensing diameter of about 1400 in wall units. This is a very large sensor relative to the "optimum" sensor size identified by Schewe [16], which is 19 wall units. The optimal size is established on several bases among which is proper evaluation of the whole set of degrees of freedom in the turbulent flow as seen in spectral analyses. The sensors in the present experiment certainly average over numerous short wavelength excitations of the fluid and sense scales which are consistent with those of the coherent structures. Indeed, on the basis of their size alone we would expect that these sensors would be responding to about ten or so coherent structures and report pressure fluctuations associated with the dynamics and interaction of this collection of coherent objects.

This qualitative picture is both consistent with and provides a rationale for the interpretation of the observations we have made in this paper when nonlinear signal processing methods [5] are applied to the data. These include:

(i) In the *ambient* data and in data taken from an *accelerometer* placed in the prow of the buoyant body we see that the mutual information "decorrelation time" of the pressure fluctuations is a factor of 2 to 3 less than the times associated with fluid dynamical motions. The dimensions of the embedding space required to unfold the attractor in the dynamics is very large and is consistent with one's usual picture of "noise."

(ii) In the data from the *laminar* flow regime of the boundary layer we also see time scales smaller than those of the fluid flow and see an embedding dimension which is very large. The laminar regime should have no pressure fluctuations, of course, so it is important to see this result as consistent with the general picture of the flow. The actual behavior of the global false nearest neighbors for these data suggests that it may be that there is a low dimensional dynamics (the beginning of Tollmien-Schlichting waves, perhaps), which is low amplitude in this region and is dominated by the ambient or instrumental "noise" seen in the ambient and accelerometer data. It is impossible with just the geometric tool of false nearest neighbors to make a decision about this possibility.

(iii) In the data in the *transition* region we see mutual information time scales that are consistent with the fluid dynamical excitations, namely about 250 μsec, and we see low dimensional embedding dimensions chosen by the data itself as needed for the unfolding of the system attractor. The Fourier spectrum in this region is consistent with a band Tollmien-Schlichting perhaps interacting with each other but now at substantially larger amplitude than might have been the case in the laminar region. The embedding dimension required for the dynamics observed through the pressure sensors is about 8 or so, varying with the individual sensor.

(iv) In the data on *turbulent* flow in the boundary layer we see much the same pattern as in the transition region. The Fourier spectra have no distinguishable Tollmien-Schlichting region, as expected, and the time scale for mutual information decorrelation is slightly larger than in the transition region, though still clearly of fluid dynamic origin. The dimension required to unfold the attractor is about 9 or 10 in this flow regime.

We did perform some computations on the Lyapunov exponents for these data using methods well established in the literature [5] but are not yet confident enough of the numerical values to report them. The issue is the ability to quantitatively do computations on Lyapunov exponents in spaces of dimension 8 to 10 using the amount of data available. The qualitative picture which consistently emerges is that there is at least one positive Lyapunov exponent as required by all descriptions of chaotic behavior and one zero exponent demonstrating that the dynamics is that of a flow, not an iterated map. The sum of all exponents was always negative, so the flow is dissipative. Finally, the order of magnitude of the largest exponent was about $(10\tau_s)^{-1}$, with $\tau_s = 15.26$ μsec, the sampling time for these data. More details on these exponents will be reported in future work.

These analyses are remarkable in providing clear evidence for low dimensional dynamics within a flow which all agree is high dimensional when all degrees of freedom are accounted for. The numerical experiments of Keefe, Moin, and Kim [6] suggest that in flows of this sort with lower-Reynolds numbers, a dimension (Lyapunov dimension) of 380 is seen. This rests on the full set of degrees of freedom excited by the flow. The present experiment has the good fortune to have utilized a sensor that averages out many of these degrees of freedom at the smallest scales and is sensitive to the dynamics and interaction of larger scale coherent structures in the boundary layer flow.

This raises the very interesting possibility for future experiments in this area: measuring the embedding (or other) dimension as a function of sensor size (in wall units). If the explanation suggested here is qualitatively correct, we would expect that as the size of the sensor is increased the embedding dimension will slowly increase as more and more coherent structures are felt by the sensor. As the sensor size is decreased, the embedding dimension will decrease until the small scale motions become of importance, and then the dimension will rise again. If this holds true, for various applications of the observations here we would suggest using the minimum of such a dimension versus sensor size curve for operating purposes.

Further, this result suggests that the idea of what dimension one will see in an extended or continuum system with intrinsically many degrees of freedom (essentially infinity in a fluid flow) depends on the resolution at which one looks. The strict notion suggested by the embedding theorem [3,4,12] that all degrees of freedom can be sensed by a single sensor of whatever size cannot be true physically unless the requirements of an infinite amount of infinitely accurate data is provided. There is a real challenge to the physical interpretation of experiments such as these to establish how dimensions will vary as sensor resolution is varied. The same question arises in the area of analysis of climate and weather. Realistic resolution in measurements appropriate for that area is typically quite coarse. This means that the many, many degrees of freedom within the primitive equations for those flows are

unlikely to be relevant to observations. The challenge of how to establish what is the relevant number of degrees of freedom as a function of resolution is what we pose here. The numerically based answer given in this paper is clearly only a bellwether stating that an interesting question is being posed.

The results in this paper suggest several directions of further inquiry:

(i) One should repeat the experiments both on the axisymmetric buoyant body and on appropriate laboratory flows. Instrumenting the body with pressure sensors of varying sizes is certainly called for as well as choosing the distribution of sensors to capture the spatial behavior of the turbulent boundary layer flows. The opportunity of using some flow visualization when possible could be very useful contribution to our understanding of these flows and measurement of the velocity and vorticity within the boundary layer in the vicinity of the pressure sensors could be quite interesting.

(ii) Using numerical simulations both existing [6] and higher resolution when possible would allow investigation of the dimension versus sensor size (effective spatial resolution) in these spatio-temporal chaotic settings. While no substitute for the real experiment, numerical experiments here have clear and well tested advantages.

(iii) One should clarify the evaluation of local and global Lyapunov exponents [5] in the spaces of dimension 8 to 10 which one must deal with in these data. The predictability associated with both local and global exponents is important to establish. Further connecting large local exponents with properties of the coherent structures would be of high physical interest.

(iv) One should develop filtering methods [5] based on models, either locally deterministic or probabilistic, for removing the effect of the observed pressure fluctuations as they serve to mask external signals of interest.

(v) Moving into the uncertain, we anticipate the use of developments of existing "control" methods for chaotic evolution [18] to allow control of the low dimensional dynamics seen in this experiment either to reduce the chaotic behavior, if that is desired, or to enhance it under other circumstances. The reduction would plausibly reduce "drag," while the enhancement might allow the use of the chaos for steering or braking of objects moving rapidly in a fluid.

ACKNOWLEDGMENTS

H.D.I.A. thanks the members of INLS for numerous discussion on this subject. His work was supported in part by the U.S. Department of Energy, Office of Basic Energy Sciences, Division of Engineering and Geosciences, under Contract No. DE-FG03-90ER14138, and in part by the U.S. Army Research Office (Contract No. DAAL03-91-C-052), and by the Office of Naval Research (Contract No. N00014-91-C-0125), under subcontract to the Lockheed/Sanders Corporation. Research at the Naval Undersea Warfare Center (NUWC) was performed under the technical direction of Richard A. Katz and was sponsored in part by the Science and Technology Directorate of NUWC, Dr. William Roderick (Special Project Initiative No. 793P13), and in part in collaboration with the USAF Foreign Aerospace Science and Technology Center, FASTC, Ms. Carolyn Schaeff (Contract No. N4175643-WX=33012).

[1] B. J. Cantwell, Annu. Rev. Fluid Mech. **13**, 457 (1981).
[2] S. K. Robinson, Annu. Rev. Fluid Mech. **23**, 601 (1991).
[3] R. Mañé, in *Dynamical Systems and Turbulence, Warwick 1980,* edited by D. Rand and L. S. Young, Lecture Notes in Mathematics Vol. 898 (Springer, Berlin, 1981), p. 230.
[4] F. Takens, in *Dynamical Systems and Turbulence, Warwick 1980,* edited by D. Rand and L. S. Young, Lecture Notes in Mathematics Vol. 898 (Springer, Berlin, 1981), p. 366.
[5] H. D. I. Abarbanel, R. Brown, J. J. Sidorowich, and L. Sh. Tsimring, Rev. Mod. Phys. **65**, 1331 (1993).
[6] L. Keefe, P. Moin, and J. Kim, J. Fluid Mech. **242**, 1 (1992).
[7] T. A. Galib and A. Zanies, NUSC Technical Memorandum No. 84-2045, 1984 (unpublished).
[8] A. E. Gentry and A. R. Wazzan, McDonnell-Douglas Report No. MDC J7255/02, 1976 (unpublished).
[9] T. A. Galib, R. Katz, S. Ko, and B. Sandman, NUSC Technical Memorandum No. 91-2083, 1991 (unpublished).
[10] T. M. Farabee and M. J. Caserella, Phys. Fluids A **3**, 2410 (1991).
[11] J.-L. Balint, J. M. Wallace, and P. Vukoslavčević, J. Fluid Mech. **228**, 53 (1991).
[12] J.-P. Eckmann and D. Ruelle, Rev. Mod. Phys. **57**, 617 (1985).
[13] A. M. Fraser and H. L. Swinney, Phys. Rev. A **33**, 1134 (1986); A. M. Fraser, IEEE Trans. Inf. Theory **35**, 245 (1989); Physica D **34**, 391 (1989).
[14] Matthew B. Kennel, R. Brown, and H. D. I. Abarbanel, Phys. Rev. A **45**, 3403 (1992).
[15] H. D. I. Abarbanel and M. B. Kennel, Phys. Rev. E **47**, 3057 (1993).
[16] G. Schewe, J. Fluid Mech. **134**, 311 (1983).
[17] E. N. Lorenz, J. Atmos. Sci. **20**, 130 (1963).
[18] E. Ott, C. Grebogi, and J. A. Yorke, Phys. Rev. Lett. **64**, 1196 (1990).

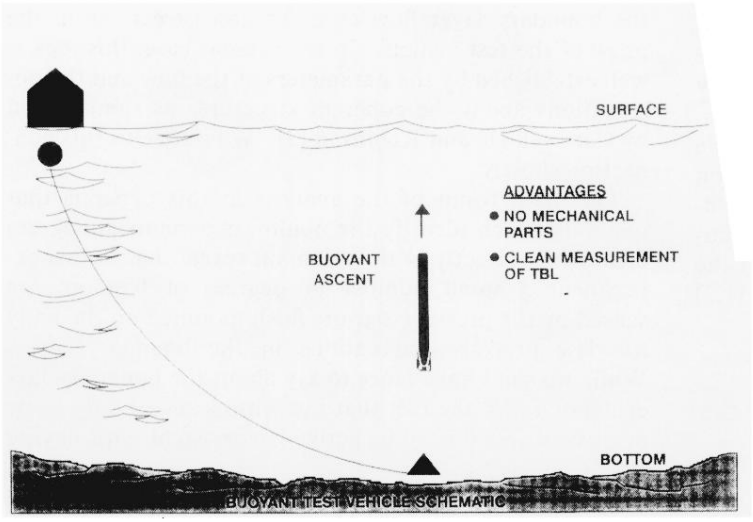

FIG. 1. The setup of the experiment on the buoyant test vehicle. The vehicle was launched at ≈ 300 m depth and rose freely to about 50 m, where it turned to avoid breaching the surface. Data were taken every 15.26 μsec for 5 sec while the vehicle was in free flight.